OH/IR stars in the inner bulge detected by ISOGAL

Ortiz, R.; Blommaert, J.A.D.L.; Copet, E.; Ganesh, S.; Habing, H.J.; Messineo, M.; ... ; Schuller, F.

A&A 388, 279–292 (2002)
DOI: 10.1051/0004-6361:20020514

Astronomy & Astrophysics

OH/IR stars in the inner bulge detected by ISOGAL⋆,⋆⋆

R. Ortiz[1,2], J. A. D. L. Blommaert[3,4], E. Copet[5], S. Ganesh[6,5], H. J. Habing[2], M. Messineo[2], A. Omont[5], M. Schultheis[5], and F. Schuller[5]

[1] Departamento de Fisica, UFES, Av. Fernando Ferrari s/n, 29060-900, Vitoria, Brazil
[2] Leiden Observatory, Niels Bohrweg 2, Postbus 9513, 2300 RA Leiden, The Netherlands
[3] ISO Data Centre, Astrophysics Division, Space Science Dept. of ESA, Villafranca, PO Box 50727, 28080 Madrid, Spain
[4] Instituut voor Sterrenkunde, K.U. Leuven, Celestijnenlaan 200 B, 3001 Leuven, Belgium
[5] Institut d'Astrophysique de Paris, CNRS, 98bis Bd. Arago, 75014, Paris, France
[6] Physical Research Laboratory, Navarangpura, Ahmedabad 380009, India

Received 3 February 2000 / Accepted 4 April 2002

Abstract. We present a study of known OH/IR stars in the inner bulge, observed by the ISOGAL survey at $\lambda = 6.8$ μm and $\lambda = 14.9$ μm. Bolometric corrections and luminosities are computed, based on near and mid-infrared data. The vast majority of the sources exhibit mass-loss rates in the range: 3×10^{-7} up to a few times 10^{-5} $M_{\odot}$/year. The bolometric magnitude distribution peaks at $M_{\rm bol} = -5.0$. There is no clear evidence that the luminosity is related to the expansion velocity of the envelope for the sample in the bulge observed by ISOGAL. We find that the bulge OH/IR stars do not follow a period-luminosity (PL) law and that they are systematically less luminous than the OH/IR extension of the PL relationship for Miras.

Key words. stars: AGB and post-AGB – stars: circumstellar matter – stars: late-type – stars: mass-loss – Galaxy: stellar content – infrared: stars

1. Introduction

The galactic bulge, especially the region near the Galactic Centre, has been scanned in search of OH 1612 MHz maser sources at high spatial resolution by various authors (Lindqvist et al. 1992a; Sevenster et al. 1997; Sjouwerman et al. 1998), using the VLA and the ATCA. On the other hand, the advent of high-quality infrared data obtained by ISOGAL (Omont et al. 2002; Omont et al. 1999a,b,c; Pérault et al. 1996) has permitted the identification of a great number of sources not previously observed in the mid-infrared range. The ISOGAL wavelengths at about 7 and 15 μm are especially suited for this purpose because: *(i)* they are little affected by interstellar extinction; *(ii)* the maximum of the spectral energy distribution of AGB stars with large mass-loss rates is situated in this wavelength range; *(iii)* the fields are not severely contaminated by foreground stars.

The ISOGAL data permit one to address key questions about the inner bulge OH/IR population, especially whether OH/IR stars in the bulge are the same as those in other parts of the Galaxy concerning their masses, luminosities and mass-loss rates.

In this work we present an infrared study of a sample of OH/IR stars compiled from the catalogues of Lindqvist et al. (1992a), Sevenster et al. (1997), and Sjouwerman et al. (1998), located in selected fields observed by the ISOGAL survey in the close vicinity of the Galactic Centre. In Sect. 2 we give a brief description of the main characteristics of the ISOGAL survey and the observations; in Sect. 3 we discuss the characteristics of the circumstellar envelopes; in Sect. 4 bolometric corrections and luminosities are presented; in Sect. 5 we discuss the existence of two distinct populations of OH/IR stars; Sect. 6 shows the use of the $K-[14.9]$ colour index as an indicator of mass-loss; in Sect. 7 the period-luminosity relationship for bulge OH/IR stars is discussed; Sect. 8 is devoted to peculiar objects.

2. ISOGAL observations

General characteristics of the ISOGAL survey have been described extensively by others (Omont et al. 2002;

Send offprint requests to: R. Ortiz,
e-mail: ortiz@cce.ufes.br

⋆ Based on observations with ISO, an ESA project with instruments funded by ESA member states.

⋆⋆ This is paper No. 6 in a refereed journal based on data from the ISOGAL project.

Schuller et al. 2002; Omont et al. 1999a,b,c; Pérault et al. 1996) and are just briefly discussed in this section.

ISOGAL observations selected for this study are those close to the Galactic Centre, obtained by using the narrow-band filters LW5 ($\lambda_{\rm ref} = 6.8$ μm, $FWHM = 0.5$ μm) and LW9 ($\lambda_{\rm ref} = 14.9$ μm, $FWHM = 2$ μm). Reduction of the data was carried out similarly as described by Schuller et al. (2002), Glass et al. (1999) and Omont et al. (1999c). After reduction, the frames were in units of ADU/gain/sec, which in turn were converted into flux density using the following relationships:

$$F(\mathrm{mJy}) = (\mathrm{ADU/gain/sec})/0.35 \quad (1)$$

for LW5 and

$$F(\mathrm{mJy}) = (\mathrm{ADU/gain/sec})/0.65 \quad (2)$$

for LW9 (Blommaert 1998), which are conversion factors assuming a $\nu \times f(\nu) = constant$ spectral shape. Colour-corrections for the narrow LW5 and LW9 filters amount to less than 1 percent for spectral index in the range –3.0 to +3.0 and have not been applied in the present study. The zero-magnitude fluxes for LW5 and LW9 are 81.8 and 17.7 Jansky respectively.

Table 1 summarizes the log-book of the observations. Cross-identification of OH sources observed by VLA provides an opportunity to check out the astrometry accuracies of infrared and radio observations. ISOGAL astrometry has been calibrated by cross-correlation with the DENIS survey (Simon et al. 2002; Epchtein et al. 1997), which in turn has its astrometry calculated from the USNO-A2 catalogue (Monet et al. 1998). The accuracy of the astrometry varies from field to field, and depends on several factors, mainly on the source density in the field, but in all cases is better than 2 arcsec. On the other hand, despite the fact that interferometric radio observations can provide *relative* positional accuracies to a fraction of an arc second, the *absolute* positions are not expected to be accurate at the one arc second level (Sjouwerman et al. 1998). A closer inspection of Table 2 of Sjouwerman et al. reveals systematic deviations between the three configurations arrays used, *a*, *b* (VLA), and *c* (ATCA). We have determined the offsets of these configurations relative to the astrometry of Lindqvist et al. (1992a), by comparing positions of the sources observed by both authors. Figure 1 shows the offsets found for each configuration. Sjouwerman's astrometry used in this paper has been corrected applying the following corrections: $\alpha_{\rm corr} = \alpha_{\rm Sj} - off(\alpha)$ and $\delta_{\rm corr} = \delta_{\rm Sj} - off(\delta)$, where $off(\alpha)$ equals to 0.5, 0.5 and 1.6 arcsec for *a*, *b* and *c* configurations and $off(\delta)$ are 4.2, 1.7 and −0.3 arcsec, respectively. It is also important to mention that positional discrepancies up to several arcseconds are reported in a few cases, even after after applying these corrections, as can be seen in Fig. 1.

The identification of ISOGAL counterparts of OH sources has been based essentially on the position criterion. A search for ISOGAL counterparts has been made in the [LW9] band, inside a 10″ radius around the radio position of double-peaked OH sources. Misidentifications are unlikely to occur, because OH/IR stars are very bright in the mid-infrared and can be easily distinguished from normal field stars. Generally, for each ISOGAL field many OH/IR stars have been identified, based on their VLA-radio position (e.g. 39 OH/IR stars identified in the TDT-82700140 observation, see Table 1).

Among the 114 OH sources searched, only 4 sources were left without a counterpart in the [LW9] and/or [LW5] band. Two of them, Li052 (OH 359.880-0.087) and Sj019 (OH 359.875-0.091), are separated by only ∼20″. The OH spectra, double peaked in both cases, and with different central velocities, −24.4 and 19 km s^{-1}, suggest that those OH emissions belong to two separate OH/IR stars.

Sj019 is probably accidentally detected as H_2O maser H_2O 359.89-0.07 by Lindqvist et al. (1990), at a velocity of 29 km s^{-1} which is consistent with the OH maser velocity. Thus Sj019 is expected to be a star.

Li52 (OH 359.880-0.087) was monitored by van Langevelde et al. (1993) who find the period of 759 days. Blommaert et al. (1998) find a very faint near-infrared counterpart for this OH source, showing $K = 18.67$ and $L_{\rm short} = 14.48$, which is by far the faintest object in the $L_{\rm short}$ band ($\lambda = 3.45$ μm) in their sample. The inspection of the images at 6.8 and 14.9 μm reveals the presence of a dark cloud in the same direction.

Sj069 (OH 0.005+0.360) was detected at 1612 MHz with the VLA by Sjouwerman et al. (1998). Its spectrum shows a single peak at the velocity of –71.2 km s^{-1}. Possibly the OH emission is of interstellar origin.

Sj102 (OH 0.317-0.066) (Sjouwerman et al., op. cit.) is moderately bright at 1612 MHz and it is double-peaked as well, showing $V_{\rm exp} = 13.1$ km s^{-1}. It was detected by ISOGAL at $\lambda = 6.8$ μm, but not at 14.9 μm. The inspection of the images at 6.8 and 14.9 μm reveals the presence of extended emission at the position of Sj102. The faint source extracted at 6.8 μm might well be a background fluctuation and not a real point source.

3. Circumstellar envelopes detected by ISOGAL

Table 2 lists the ISOGAL detections and the photometry. The ordering refers to the original paper where the OH source was taken from. When there are several ISOGAL observations with the same filter (LW5 or LW9), the average of the ISOGAL magnitudes in that filter is given.

Figure 2 shows a map of ISOGAL counterparts of the OH sources. Sources observed by Blommaert et al. (1998) as well as the ones monitored by Wood et al. (1998) are shown. The region very near the Galactic Centre was not observed in the ISOGAL survey to avoid saturation of the ISOCAM detector (Césarsky et al. 1996).

Figure 3 shows the [LW5] vs. [LW5]−[LW9] colour-magnitude diagram for all OH/IR sources detected in these two bands, together with the other infrared sources from the selected fields (not identified as OH/IR stars).

Table 1. ISOGAL Fields in which counterparts of the OH maser sources have been found. The *TDT* names are the usual basic reference to individual ISO observations. The names of the fields are the coordinates of its center; Δl and Δb are the approximate semi-widths of the fields; and N is the number of counterparts found in the field.

		LW5 ($\lambda = 6.8$ μm) band				LW9 ($\lambda = 14.9$ μm) band				
Field	#	TDT name	$\Delta l(^\circ)$	$\Delta b(^\circ)$	Obs. Date	TDT name	$\Delta l(^\circ)$	$\Delta b(^\circ)$	Obs. Date	N
$-01.12-00.33$	1	-	-	-	-	31300313	0.31	0.19	24-Sep.-1996	1
$-00.90-00.03$	2	31300837	0.30	0.17	25-Sep.-1996	83800857	0.20	0.17	02-Mar.-1998	4
$-00.81-00.15$	3	-	-	-	-	84300221	0.18	0.07	07-Mar.-1998	1
$-00.81-00.15$	4	-	-	-	-	49101221	0.18	0.07	21-Mar.-1997	1
$-00.62-00.06$	5	31300236	0.16	0.17	24-Sep.-1996	83600308	0.11	0.17	28-Feb.-1998	4
$-00.34+00.18$	6	-	-	-	-	31300901	0.39	0.09	25-Sep.-1996	14
$-00.27-00.03$	7	-	-	-	-	83801051	0.03	0.08	02-Mar.-1998	3
$-00.27-00.03$	8	31300135	0.16	0.17	24-Sep.-1996	82700140	0.16	0.17	19-Feb.-1998	39
$+00.00+01.00$	9	83600419	0.15	0.06	28-Feb.-1998	83600524	0.15	0.06	28-Feb.-1998	1
$+00.04+00.40$	10	-	-	-	-	13600318	0.40	0.13	01-Apr.-1996	4
$+00.05-00.24$	11	83600855	0.16	0.13	28-Feb.-1998	83600856	0.16	0.13	28-Feb.-1998	15
$+00.34-00.05$	12	31300734	0.14	0.15	25-Sep.-1996	82800341	0.13	0.15	20-Feb.-1998	18
$+00.37+00.17$	13	84100143	0.30	0.09	05-Mar.-1998	13600503	0.30	0.09	01-Apr.-1996	9
$+00.59+00.02$	14	31300433	0.14	0.15	24-Sep.-1996	83800712	0.13	0.09	02-Mar.-1998	2
$+00.62-00.14$	15	31300433	0.14	0.15	24-Sep.-1996	84100259	0.12	0.07	05-Mar.-1998	4

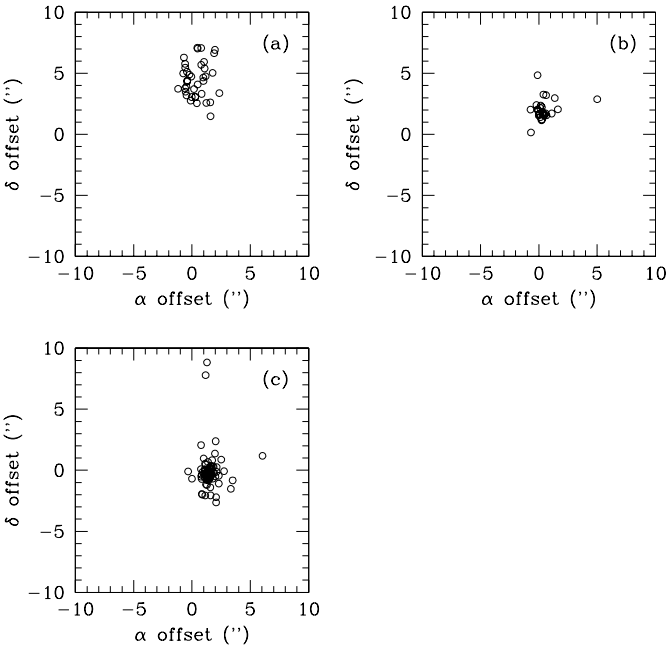

Fig. 1. Astrometric deviations: *Sjouwerman − Lindqvist* coordinates. The offsets for a, b (VLA), and c (ATCA) configurations are shown. See Sjouwerman et al. (1998) for a description of the a and b modes.

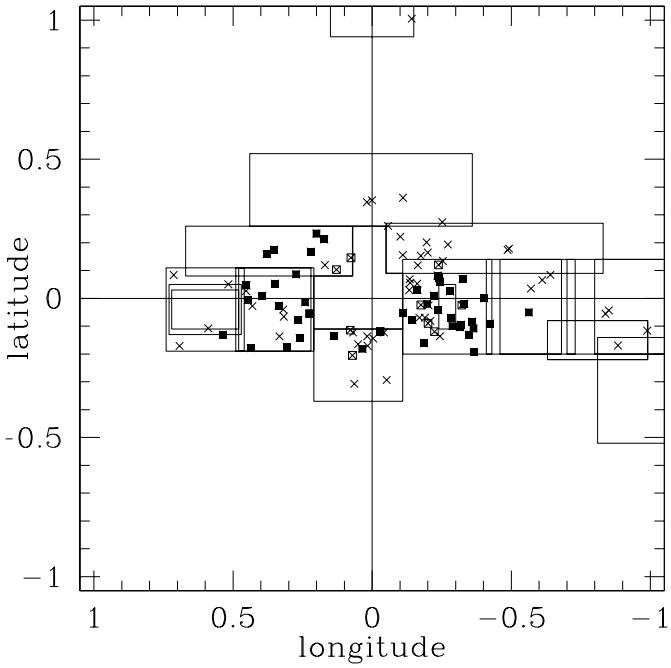

Fig. 2. Map of OH sources in the bulge: ISOGAL detections in two bands (crosses); sources detected by ISOGAL and observed by Blommaert et al. (1998) (open squares); sources detected by ISOGAL and monitored by Wood et al. (1998) (filled squares). The rectangles show the limits of the ISOGAL fields searched, listed in Table 1.

The OH/IR stars occupy the upper part of the diagram, showing luminosities higher than most field sources. An upper limit of luminosity is well defined, at [LW5] $\simeq$3.0. Above it, four objects are separated by a gap, which are either foreground objects or intrinsically very luminous. They are discussed in Sect. 8.

In the same diagram we plot the results of a model of circumstellar dust shell developed by Groenewegen (1993). The models assume $L = 5000\ L_\odot$ ($M_{\rm bol} = -4.5$), distance of 7.9 kpc and the dust-to-gas ratio of 1/200. The dust opacity assumed is that of David & Papoular (1990, 1992), but with the 9.8 μm feature artificially removed and with $\tau_V = 18.6 \times \tau_{10.2}$. The removal of the silicate feature is not important in this study, since it is out of range of the [LW5] and [LW9] filters. Sequences of increasing mass-loss rates are displayed for M5III and M8III spectral types in the mass-loss range $10^{-8} \sim 10^{-5}\ M_\odot$/year (see Sect. 6).

Table 2. ISOGAL counterparts of double-peaked OH sources at $\lambda = 6.8$ and 14.9 μm. The ordering refers to the original paper where the OH source was taken from. Field # 's are listed in Table 1. Peculiar OH spectra are denoted by *pec.* OH in the last column. The references for periods and bolometric magnitudes in the two last columns are: △ = Wood et al. (WHMc, 1998); ♡ = van Langevelde et al. (1993), and ♢ = Jones et al. (1994). Peculiar objects concerning photometry (very red, bright or faint) are discussed in Sect. 8.

Name	OH name	ISOGAL PJ	[LW5]	[LW9]	Field #	P(days)	Comments
Li001	OH 359.360+0.084	174345.5-292619	4.06	2.14	5		
Li002	OH 359.388+0.066	174354.2-292523	4.48	1.80	5		
Li003	OH 359.429+0.035	174406.9-292417	7.26	3.08	5		very red source, pec.OH
Li004	OH 359.437-0.051	174428.3-292635	6.53	4.24	5		faint object
Li009	OH 359.508+0.179	174344.8-291544	non-obs	2.86	6	644△	
Li010	OH 359.513+0.174	174346.8-291538	non-obs	3.59	6	461△	
Li012	OH 359.576-0.091	174457.8-292042	4.66	2.45	8	672△	
Li014	OH 359.598+0.000	174439.7-291645	4.50	2.35	8	664△	
Li016	OH 359.634-0.195	174530.5-292059	4.98	3.09	8	501△	
Li017	OH 359.636-0.108	174510.5-291811	3.98	1.80	8	847△	
Li018	OH 359.640-0.084	174505.3-291713	4.21	2.73	8	546△	
Li019	OH 359.652-0.131	174518.1-291804	5.91	4.32	8	671△	
Li020	OH 359.669-0.019	174454.2-291344	4.89	3.23	8	481△	
Li021	OH 359.675+0.069	174434.4-291038	4.05	1.76	8	698△	pec.OH
Li022	OH 359.678-0.024	174456.9-291325	3.14	2.06	8	645♢	$M_{\rm bol} = -6.17$♢
Li023	OH 359.681-0.095	174514.0-291527	3.47	1.59	8	759△	
Li024	OH 359.684-0.104	174516.5-291537	4.60	3.48	8	535△	
Li025	OH 359.711-0.100	174519.4-291405	4.08	2.05	7,8	686△	
Li026	OH 359.716-0.070	174513.0-291254	3.49	2.64	7,8	691△	
Li027	OH 359.719+0.025	174451.3-290945	4.44	2.86	7,8	669△	
Li029	OH 359.746+0.134	174429.5-290458	5.48	3.69	6,8	395♢	$M_{\rm bol} = -4.90$♢
Li030	OH 359.748+0.274	174357.1-290028	non-obs	3.17	10	437△	
Li031	OH 359.755+0.061	174448.0-290649	5.03	2.85	8	No period♡	
Li032	OH 359.760+0.072	174446.0-290613	3.17	2.37	8	676△	
Li033	OH 359.762+0.120	174435.0-290435	1.74	0.27	6,8	758♡	bright IR source
Li034	OH 359.763-0.042	174513.1-290936	4.29	2.83	8	453△	
Li035	OH 359.765+0.082	174444.5-290538	3.57	2.05	8	552△	
Li037	OH 359.776-0.120	174533.3-291123	5.34	3.81	8	No period♢	$M_{\rm bol} = -3.40$♢
Li038	OH 359.778+0.010	174503.2-290712	4.83	3.53	8	557△	
Li040	OH 359.799-0.090	174529.5-290916	4.87	3.06	8	610♢	$M_{\rm bol} = -4.80$♢
Li041	OH 359.800+0.165	174430.2-290114	non-obs	2.86	6	461△	
Li042	OH 359.803-0.021	174514.0-290656	3.35	2.23	8	838△	
Li044	OH 359.810-0.070	174526.4-290804	4.63	2.69	8	640♢	$M_{\rm bol} = -5.35$♢
Li045	OH 359.814-0.162	174548.5-291045	4.90	3.52	8	554△	
Li046	OH 359.825+0.153	174436.5-290019	non-obs	2.03	6	493△	
Li047	OH 359.825-0.024	174517.9-290553	4.19	2.91	8	650♢	$M_{\rm bol} = -5.80$♢
Li048	OH 359.837+0.030	174507.0-290334	4.86	2.73	8	402△	
Li050	OH 359.855-0.078	174534.8-290602	3.56	2.55	8	617△	
Li054	OH 359.889+0.361	174357.0-285030	non-obs	3.20	10	389△	
Li055	OH 359.890+0.155	174445.0-285657	non-obs	3.04	6	568△	No period♡
Li056	OH 359.899+0.222	174431.0-285424	non-obs	1.47	6	No period♡	
Li064	OH 359.943+0.260	174428.2-285055	non-obs	2.09	6	692△	
Li070	OH 359.971-0.119	174601.1-290124	2.30	0.68	11	1391♡	bright IR source
Li071	OH 359.974+0.162	174455.7-285227	non-obs	3.12	6	636△,712♡	
Li074	OH 359.966-0.144	174610.4-290043	4.18	2.18	11		
Li076	OH 0.001+0.352	174415.0-284505	non-obs	2.04	10	477△	
Li078	OH 0.018+0.156	174503.3-285022	non-obs	5.70	6	423△	
Li079	OH 0.019+0.345	174419.3-284421	non-obs	1.52	10	701△	
Li080	OH 0.036-0.182	174624.8-290002	4.72	2.89	11	660△	
Li085	OH 0.071-0.205	174635.6-285901	4.26	2.35	11	770♢	$M_{\rm bol} = -4.90$♢
Li086	OH 0.076+0.146	174513.9-284743	3.43	1.52	13	639♡	$M_{\rm bol} = -5.73$♢
Li087	OH 0.079-0.114	174615.4-285542	3.24	1.64	11	700♢	$M_{\rm bol} = -5.05$♢
Li091	OH 0.129+0.103	174531.5-284622	4.87	3.69	13	480♢	$M_{\rm bol} = -5.15$♢
Li094	OH 0.138-0.136	174628.8-285319	4.54	2.73	11	622△	
Li096	OH 0.173+0.211	174512.5-284044	4.68	1.45	13	514△	very red source

Table 2. continued.

Name	OH name	ISOGAL PJ	[LW5]	[LW9]	Field #	P(days)	Comments
Li101	OH 0.200+0.233	174511.5-283843	3.44	1.50	13	825△	
Li104	OH 0.221+0.168	174529.1-283938	4.55	2.59	13	697△	
Li105	OH 0.225-0.055	174622.2-284622	3.84	1.97	12	521△	
Li106	OH 0.241-0.014	174615.0-284417	4.56	3.07	12	535△	
Li107	OH 0.261-0.143	174647.9-284715	5.72	3.50	12	No period△	faint object, pec.OH
Li108	OH 0.265-0.078	174633.1-284500	4.89	4.04	12	595△	
Li109	OH 0.274+0.086	174556.1-283926	3.60	1.89	12,13	706△	
Li110	OH 0.307-0.176	174702.2-284555	4.32	2.88	12	657△	
Li111	OH 0.319-0.040	174632.2-284104	4.66	1.53	12	No period♡	very red source, pec.OH
Li112	OH 0.333-0.137	174656.7-284322	4.84	3.17	12		
Li113	OH 0.336-0.027	174631.3-283948	4.86	3.09	12	514△	
Li114	OH 0.349+0.053	174614.5-283639	4.28	3.29	12	669△	
Li115	OH 0.352+0.175	174546.6-283240	3.36	1.82	13	661△	
Li116	OH 0.379+0.159	174554.2-283146	3.85	1.75	13	985△	
Li117	OH 0.395+0.008	174631.8-283540	4.56	3.11	12	461△	
Li118	OH 0.430-0.027	174645.0-283502	4.70	2.49	12		
Li119	OH 0.437-0.179	174721.3-283923	3.64	1.88	12	744△	
Li120	OH 0.447-0.006	174642.3-283326	4.74	3.98	12	445△	
Li121	OH 0.452+0.046	174630.7-283131	7.03	5.77	12	339△	faint object
Li122	OH 0.453+0.026	174635.7-283208	4.30	3.55	12		
Li125	OH 0.517+0.050	174639.1-282806	5.01	4.70	14		
Li126	OH 0.523-0.206	174739.8-283549	non-obs	2.20	15	1050△	ISOGAL position uncertain
Li127	OH 0.536-0.130	174724.1-283243	3.48	2.12	15	669△	
Li130	OH 0.589-0.108	174726.3-282920	5.73	5.30	15		
Li131	OH 0.692-0.171	174755.6-282602	6.18	5.30	15		
Li132	OH 0.713+0.084	174659.1-281658	4.06	1.67	14		
Sj001	OH 359.728+0.193	174413.1-290403	non-obs	2.36	6		
Sj002	OH 359.757-0.136	174534.4-291254	4.30	2.71	8		
Sj003	OH 359.791-0.081	174526.3-290924	3.99	2.75	8		
Sj004	OH 359.797-0.025	174514.3-290720	4.14	2.40	8		
Sj006	OH 359.805+0.200	174422.4-285954	non-obs	2.62	6		
Sj008	OH 359.830-0.070	174529.3-290704	4.40	2.96	8		
Sj009	OH 359.836+0.119	174446.0-290051	4.28	2.85	6,8		
Sj011	OH 359.838+0.053	174501.7-290249	4.91	3.26	8	469♡	
Sj013	OH 359.864+0.056	174504.8-290124	5.52	3.86	8		
Sj014	OH 359.864+0.068	174501.8-290055	5.22	4.01	8		
Sj016	OH 359.867+0.029	174511.3-290203	4.46	2.95	8		
Sj018	OH 359.869-0.018	174522.8-290331	5.16	2.29	8		
Sj031	OH 359.936-0.145	174602.8-290359	5.90	2.52	11		very red source
Sj041	OH 359.947-0.294	174638.5-290803	4.66	2.73	11		
Sj047	OH 359.957-0.123	174559.9-290211	6.14	5.30	11		
Sj073	OH 0.015-0.171	174619.6-290041	4.89	2.67	11		
Sj075	OH 0.017-0.137	174611.7-285932	5.23	3.96	11		
Sj087	OH 0.050-0.165	174623.0-285845	5.07	3.06	11		
Sj090	OH 0.064-0.308	174658.5-290227	4.96	3.33	11		
Sj092	OH 0.067-0.123	174615.8-285632	5.30	3.40	11		
Sj100	OH 0.121-0.112	174620.7-285329	5.08	2.92	11		
Sj101	OH 0.170+0.119	174533.2-284348	4.00	2.16	13		
Sj102	OH 0.317-0.066	174637.7-284151	7.08	non-det	12		strong background emission
Se126	OH 359.857+01.00	174122.7-283146	3.62	1.55	9		
Se144	OH 359.011-00.11	174342.0-295021	4.75	2.22	2		
Se145	OH 359.149-00.04	174345.0-294101	1.97	-0.75	2		bright IR source
Se147	OH 359.161-00.05	174349.6-294044	3.49	2.49	2		
Se151	OH 359.117-00.16	174409.9-294639	2.34	1.02	4,3,2,1		bright IR source
Se179	OH 000.333-00.18	174707.0-284442	non-obs	3.10	12		

OH/IR stars are concentrated near the steepest part of the curves, corresponding to mass-loss rate between $10^{-7} \sim 10^{-5}$ $M_{\odot}$/year. The model predicts luminosities which match well with the observations, but the observed colours are spread over a much wider range. This discrepancy might be (partially) explained by variability: sources which had photometry obtained simultaneously in the two bands follow the curves more closely than those observed in different epochs. Infrared variability at these wavelenghts has been previously reported by Harvey et al. (1974) who monitored OH/IR stars in several infrared bands. They studied the amplitudes of variability in several photometric bands, including a broad band ranging from 8 to 13 μm, which is close to [LW5] and [LW9] ISOGAL bands. Their average value of the amplitude of the light curve at $\lambda \sim 10$ μm is 0.9, and the range is from 0.3 up to 1.7 mag, which is approximately the same dispersion in colour seen in Fig. 3.

A significant number of infrared sources without detected OH emission, is found in the same part of the colour-magnitude diagram as the OH/IR stars (see also Schuller et al. 2002). Infrared sources showing colours typical of O-rich, high mass-losing stars, but without 1612 MHz emission have been reported in the literature as "colour mimics" by Lewis & Engels (1993). They might amount up to 40 per cent, but this number varies according to the place in the Galaxy, being lower towards the bulge (Le Squeren et al. 1992; Blommaert et al. 1993). The detection rate depends also on the observing conditions: Sjouwerman et al. (1998) surveyed with more sensitivity the area formerly covered by Lindqvist et al. and found many new OH masers previously undetected, formerly considered as *mimics*. Variability of the OH emission might also play a role: it is well known that the OH emission follows the same variability pattern as the infrared light curve (Harvey et al. 1974), and consequently OH/IR stars in the faint phase of the cycle might be more difficult to detect.

We also looked for IRAS counterparts of OH/IR stars in the inner bulge, but those data are mostly of poor quality, due mainly to "confusion". Only one IRAS source which could be associated with a source of this study (IRAS17419-2907, which coincides with Li34) has moderate-to-good quality fluxes in the [12], [25] and [60] bands; it is very probably a young stellar object. A few good-quality IRAS data are considered in the discussion of individual objects in Sect. 8.

4. Bolometric corrections and luminosities

Blommaert et al. (1998, hereafter BVLHS) obtained near- and mid-infrared photometry of 34 sources, some of them previously monitored by van Langevelde et al. (1993) in the OH frequency. Wood et al. (1998, hereafter WHMc) monitored 86 OH/IR stars in the K band and obtained JHL photometry as well. This was mostly aimed at stars not included in the list of targets by van Langevelde et al. In this study, we combine the near-infrared photometry

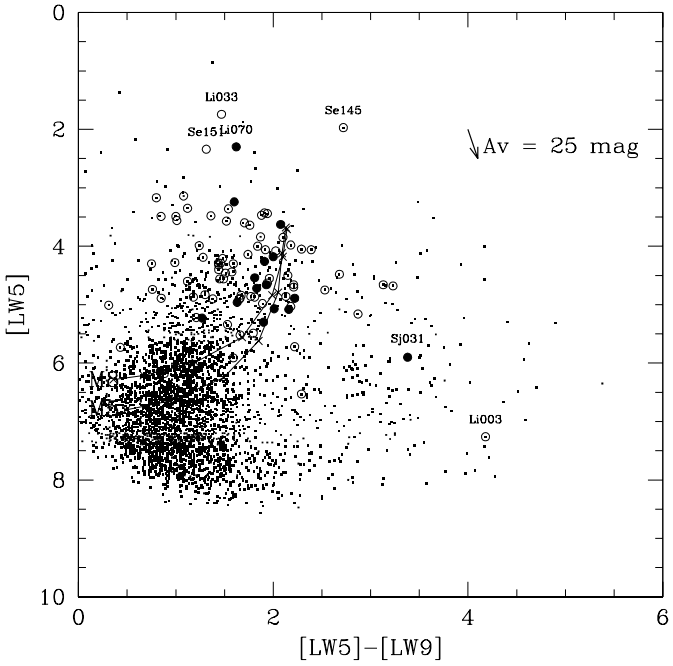

Fig. 3. Colour-magnitude diagram for ISOGAL OH/IR stars. Black circles: OH/IR stars with simultaneous two-filter measurements; open circles: OH/IR stars measured at different epochs; dots: ISOGAL sources in the field $-00.27 - 00.03$, shown just for comparison. The curves represent the predictions of a model for circumstellar dust shells developed by Groenewegen (1993). Mass loss ranges from 1×10^{-8} up to 1×10^{-5} $M_{\odot}$/year: it increases from left to upper right and the ticks represent steps of half a dex. Sources in this diagram have not been corrected for extinction.

obtained by WHMc and BVLHS with that of ISOGAL. Only two sources were observed both by WHMc, BVLHS and ISOGAL. For sources observed both by WHMc and BVLHS we adopt WHMc photometry, since it refers to an *average* K magnitude.

To obtain bolometric magnitudes $M_{\rm bol}$ we integrated the flux densities over wavelength, between 1.25 μm $< \lambda <$ 14.9 μm, using the trapezium method and added two extra terms: *(i)* $F_{<1.25}$, the flux radiated at $\lambda < 1.25$ μm; *(ii)* $F_{>14.9}$, corresponding to the flux radiated beyond $\lambda = 14.9$ μm. $F_{<1.25}$ is significant only for two sources: Li4 and Li18, which have near-infrared colour temperatures of 3630 and 3330 K respectively $F_{<1.25}$ is calculated by fitting a blackbody to the near-infrared flux densities. However, these temperatures are uncertain because of observations at different epochs. The inclusion of $F_{>14.9}$ is performed as follows: the spectral index α, defined as $f(\nu) \propto \nu^{+\alpha}$, between 6.8 and 14.9 μm is given by:

$$\alpha = 1.89 - 1.16 \times ([LW5] - [LW9]). \quad (3)$$

Table 2 and Fig. 3 show that $[LW5] - [LW9] \simeq 2$ on average, which gives $\alpha \simeq -0.4$. This means that the energy distribution is still rising between 6.8 and 14.9 μm for most sources. In order to estimate $F_{>14.9}$, we have fitted a blackbody with colour temperature $T_{6.8-14.9}$ on ISOGAL flux densities at 6.8 and 14.9 μm. A test showed that

integration of the flux densities on frequency, instead of wavelength, produces the same results within 0.02 mag accuracy.

Before integration, all flux densities were corrected for interstellar extinction. The visual extinction was obtained by two methods: *(i)* the reddening derived by WHMc is converted into visual extinction using the relationship: $A_{\rm V} = 16.7 \times E(H-K)$ (Glass 1999); *(ii)* the visual extinction derived by Schultheis et al. (1999), obtained by fitting theoretical isochrones to RGB and AGB stars, in the $(J-K)\times K_{\rm s}$ diagram. WHMc calculated the $E(H-K)$ for each field $(1'\times 1')$ comparing the observed colours with intrincisic $H-K$ colour of red giants. Schultheis et al. (1999) used for each cell size (2′/pixel) the DENIS $K_{\rm s}$ vs. $(J-K_{\rm s})$ diagrams together with theoretical isochrones for the RGB/AGB population. Due to the limited sensitivity of DENIS, their map is only reliable up to $A_{\rm V} < 25^{\rm m}$.

Figure 4 shows the comparison between both determinations of $A_{\rm V}$. There is no systematic deviation between the two methods, however there is a large scatter with a rms of ∼7 mag in $A_{\rm V}$. Nearly all sources lie inside the 25% discrepancy region, indicated by the dashed lines in Fig. 4. A simulation showed that, for 25% of uncertainty in $A_{\rm V}$, the uncertainty in the determination of $M_{\rm bol}$ is about 0.5 magnitude for $(K-L)_{\rm o} \lesssim 1.5$ and 0.2 magnitude for $(K-L)_{\rm o} \gtrsim 1.5$. The only exceptions in the sample are Li4 and Li18, which have optically thin envelopes. For these stars 25% of uncertainty in $A_{\rm V}$ causes one magnitude of uncertainty in $M_{\rm bol}$. We choose to take the average value of both determinations of $A_{\rm V}$.

A_λ was obtained from $A_{\rm V}$ assuming $A_J/A_{\rm V} = 0.245$, $A_H/A_{\rm V} = 0.142$, $A_K/A_{\rm V} = 0.089$, $A_L/A_{\rm V} = 0.039$ (Glass 1999). The value of the average interstellar extinction in the LW5 and LW9 bands is still uncertain (see e.g. Lutz et al. 1996; Lutz 1999; Bertoldi et al. 1999). We use the values of Mathis (1990): $A_{\rm LW5}/A_{\rm V} = 0.020$ and $A_{\rm LW9}/A_{\rm V} = 0.016$. In a simulation, we found that if one doubles these extinction coefficients, the bolometric magnitude becomes only 0.3 mag brighter.

Besides extinction, another major source of uncertainty in the luminosity calculus is variability. To derive the uncertainty of the average luminosity, it is necessary to obtain the amplitude of variability over a wide range of wavelengths, as well as to extrapolate the values of amplitude to the far-infrared. We studied the sample of OH/IR stars monitored by WHMc and Harvey et al. (1974) in order to estimate the uncertainty of $M_{\rm bol}$ caused by variability. The half-amplitude of variability is 0.9 mag at $\lambda = 2.2$ μm (WHMc), and 0.5 mag at $\lambda = 10$ μm (Harvey et al. 1974). Since OH/IR stars radiate mostly beyond $\lambda \simeq 2$ μm and the amplitude of variability seems to decrease with wavelength, we estimate the uncertainty of bolometric magnitude to be *less* than one magnitude.

In this work we adopt the distance modulus of $(m-M) = 14.5$, corresponding to the distance of 7.9 kpc (Rohlfs & Kreitschmann 1987). The choice of the distance modulus of the Galactic Centre is a minor source of uncertainty, compared with variability of the sources and the uncertainty in the extinction. The depth of the spatial distribution of OH/IR stars in the inner bulge plays a minor role in the uncertainty of the distances as well: the spatial distribution of the OH/IR stars found by Sjouwerman et al. and Lindqvist et al. shows that most sources found in these surveys are distributed in the sky like a cluster of OH sources inside the ∼20′ (∼50 parsecs) radius area, centered approximately at the Galactic Centre (see Fig. 2).

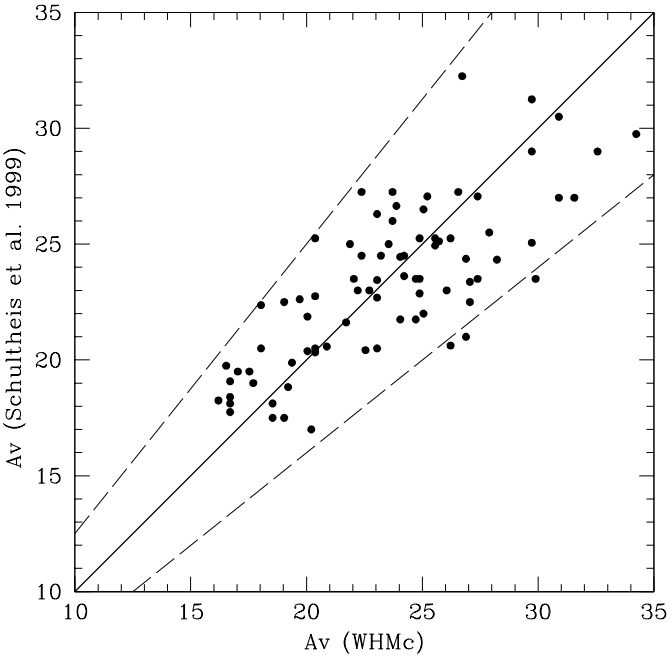

Fig. 4. Comparison between the interstellar extinction towards OH/IR sources, as derived by Schultheis et al. (1999) and by WHMc. The dashed lines represent 25% deviation from correspondence.

Table 3 lists the visual extinction $A_{\rm V}$, dereddened $(K-L)_{\rm o}$, $M_{\rm bol}$, bolometric corrections for K, L, [LW5] and [LW9] bands (all of them corrected for extinction), the $T_{6.8-14.9}$ blackbody colour temperature, and ΔV, the difference of velocity of the two OH velocity peaks. We stress that $T_{6.8-14.9}$ is not the temperature of the circumstellar dust shell, but the fit of a blackbody function to the ISOGAL flux densities, which are the outcome of radiative processes in the circumstellar envelope, such as dust absorption and emissivity. Although the thermal contribution of dust dominates at those wavelengths, a significant contribution from the atmosphere of the star might play a role, especially for optically thinner envelopes at 6.8 μm.

Table 4 contains stars observed by BVLHS. Their K, L' (differently from WHMc, L' centered at $\lambda = 3.8$ μm) and M (at 4.7 μm) magnitudes as well as ISOGAL measurements are used to compute bolometric magnitudes.

The bolometric correction is defined here, as usual, as $M_{\rm bol}(\lambda) = M_\lambda + BC_\lambda$ for a photometric band centered at λ. Figure 5 shows bolometric corrections for various bands as a function of $(K-L)_{\rm o}$, for WHMc sources. Among the photometric bands used in this study, BC_K is the only one that fits close the $(K-L)_{\rm o}$ colour (Fig. 5a), similarly to the

Table 3. Bolometric magnitudes and corrections for Lindqvist OH sources observed by Wood et al. (1998). The numbering is taken from the original reference (Lindqvist et al. 1992a); $T_{6.8-14.9}$ is the blackbody colour temperature calculated by fitting a blackbody to ISOGAL flux densities; ΔV is the difference of the two OH velocity peaks; and $M_{\rm bol}$(WHMc) is the bolometric magnitude calculated by Wood et al. (1998). The $(K-L)_{\rm o}$ colour index as well as the various bolometric corrections have been dereddened as described in Sect. 4.

No.	$A_{\rm V}$	$(K-L)_{\rm o}$	$M_{\rm bol}$	BC_K	BC_L	$BC_{\rm LW5}$	$BC_{\rm LW9}$	$T_{6.8-14.9}$(K)	ΔV km s^{-1}	$M_{\rm bol}$(WHMc)
4	29.6	0.40	−3.6	2.08	2.47	4.96	7.13	420.	30.6	−3.36
12	24.2	2.99	−4.3	1.54	4.53	6.03	8.15	430.	37.2	−4.80
14	23.4	2.77	−4.3	1.49	4.26	6.22	8.27	440.	38.4	−4.32
16	23.5	2.56	−4.2	2.15	4.71	5.83	7.63	490.	-	−4.60
17	22.0	3.98	−4.8	0.54	4.52	6.13	8.22	430.	44.2	−5.96
18	22.0	1.09	−6.7	2.33	3.42	3.99	5.38	590.	27.2	−6.00
19	20.2	3.06	−2.3	0.37	3.43	6.72	8.23	560.	40.8	−1.68
20	23.0	1.21	−4.8	3.07	4.28	5.24	6.81	540.	34.9	−4.80
21	20.9	3.68	−4.6	0.54	4.22	6.24	8.44	420.	37.5	−5.24
23	23.3	3.43	−5.0	0.40	3.82	6.55	8.33	490.	42.0	−4.98
24	22.6	1.54	−5.3	2.83	4.37	5.06	6.09	740.	32.6	−5.20
25	23.0	1.86	−5.0	2.57	4.43	5.85	7.79	460.	38.5	−5.17
26	24.5	2.41	−5.1	1.95	4.36	6.42	7.17	940.	44.2	−5.18
27	24.8	2.71	−4.0	1.27	3.98	6.55	8.03	570.	45.4	−3.78
31	19.7	0.65	−4.1	2.73	3.38	5.75	7.85	430.	37.5	−3.87
32	20.9	3.75	−5.1	0.59	4.34	6.61	7.33	970.	38.3	−5.93
34	23.2	1.83	−4.8	2.46	4.30	5.90	7.27	600.	28.4	−4.67
35	18.6	3.37	−4.8	0.93	4.30	6.46	7.90	570.	31.8	−5.30
38	24.7	1.85	−4.2	2.67	4.53	5.97	7.17	660.	42.0	−4.35
42	23.0	5.03	−4.7	−1.65	3.38	6.87	7.90	740.	44.2	−5.57
45	26.2	1.95	−4.4	2.70	4.65	5.68	6.95	630.	40.9	−4.68
48	22.0	1.30	−4.8	2.81	4.11	5.25	7.29	440.	14.5	−4.62
50	20.1	2.47	−5.2	2.09	4.56	6.19	7.12	800.	43.1	−5.37
70	25.3	4.22	−5.8	−3.83	0.39	6.90	8.42	550.	38.6	−2.98
80	28.5	3.37	−4.3	1.38	4.75	6.01	7.72	500.	37.5	−5.17
94	25.9	1.78	−5.2	2.83	4.61	5.33	7.03	510.	40.8	−5.32
96	16.8	2.01	−4.9	2.39	4.40	5.22	8.39	310.	34.1	−4.90
101	17.7	4.06	−4.8	−0.57	3.50	6.61	8.47	470.	31.6	−4.96
104	16.6	3.62	−4.3	1.09	4.72	6.01	7.90	470.	38.3	−5.34
105	25.2	2.43	−4.9	1.87	4.31	6.22	7.99	490.	32.9	−4.90
106	24.2	1.19	−5.0	2.96	4.15	5.47	6.86	590.	37.4	−4.84
107	22.6	2.69	−2.7	0.24	2.93	6.56	8.69	430.	9.1	−1.45
108	29.4	2.10	−4.2	2.50	4.61	6.04	6.78	960.	36.2	−4.31
109	17.3	2.92	−4.7	0.90	3.82	6.57	8.21	520.	48.8	−4.39
110	20.8	2.60	−4.5	1.98	4.58	6.14	7.50	600.	40.8	−4.76
113	24.5	1.24	−4.8	3.07	4.31	5.34	7.01	510.	34.0	−4.83
114	22.1	3.57	−3.8	0.04	3.61	6.83	7.74	820.	28.4	−3.69
115	17.5	2.32	−5.0	1.72	4.04	6.49	7.96	570.	36.3	−4.65
116	17.7	3.95	−5.4	1.07	5.03	5.60	7.63	440.	30.6	−7.01
117	18.9	3.16	−3.7	0.87	4.03	6.58	7.96	600.	26.1	−3.81
119	24.3	3.48	−4.8	0.40	3.88	6.58	8.24	520.	35.2	−4.87
120	22.3	2.11	−3.5	1.80	3.91	6.68	7.35	1020.	26.1	−3.10
121	17.6	0.26	−2.8	3.65	3.91	5.04	6.23	670.	20.4	−4.62
127	23.8	1.88	−5.4	2.48	4.36	6.14	7.40	640.	46.5	−5.40

one obtained with $(K-[12])_{\rm o}$ (e.g., Groenewegen 1997). The bolometric corrections for L, [LW5] and [LW9] bands are little colour dependent. Nevertheless BC_L shows a plateau, near $BC_L = 4 \sim 5$, whereas WHMc's fit for this band turns down for $(K-L)_{\rm o} > 2$.

In Fig. 6 we show a comparison between bolometric magnitudes determined in this work and those derived by WHMc and BVLHS. Our results agree within 0.6 mag accuracy with those of BVLHS, and no systematic deviation is found over the whole range of $M_{\rm bol}$. On the other hand, WHMc magnitudes are systematically brighter, for some sources by as much as 1.5 mag. The methods used in the three works are not the same: WHMc calculated $M_{\rm bol}$ applying a bolometric correction BC_L to $L_{\rm o}$, the extinction corrected L, while BVLHS preferred to integrate over the energy distribution, similarly to the present work, but

Table 4. Bolometric magnitudes and corrections for Lindqvist OH sources observed by Blommaert et al. (1998) and detected by ISOGAL. The columns are defined like in Table 3, except that here the L' band is used which is centered at $\lambda = 3.8$ μm.

No.	A_V	$(K-L')_o$	M_{bol}	BC_K	$BC_{L'}$	BC_{LW5}	BC_{LW9}	$T_{6.8-14.9}$(K)	ΔV km s^{-1}	M_{bol}(BVLHS)
22	23.5	2.11	−5.8	4.85	5.02	6.00	6.99	770.	43.1	−5.6
33	19.0	3.46	−6.7	4.77	5.18	6.42	7.81	590.	30.6	−6.5
37	26.6	4.37	−3.0	4.14	5.11	6.67	8.09	580.	27.0	−2.9
40	22.5	3.53	−3.9	5.08	5.20	6.13	7.85	500.	36.3	−4.0
47	25.0	2.93	−4.8	5.10	5.37	6.04	7.22	670.	42.8	−5.2
70	25.3	7.44	−5.8	2.69	4.19	6.88	8.40	550.	38.6	−6.0
85	24.3	4.91	−4.3	3.55	5.71	6.46	8.28	480.	27.3	−4.6
86	23.1	3.24	−5.0	4.21	4.55	6.55	8.37	480.	42.0	−5.0
87	24.8	4.72	−4.8	2.07	3.31	6.94	8.44	560.	28.3	−4.1
91	19.3	1.56	−4.6	4.72	4.71	5.38	6.48	710.	22.7	−4.0
105	25.2	2.97	−4.7	4.43	4.91	6.43	8.20	490.	32.9	−5.0

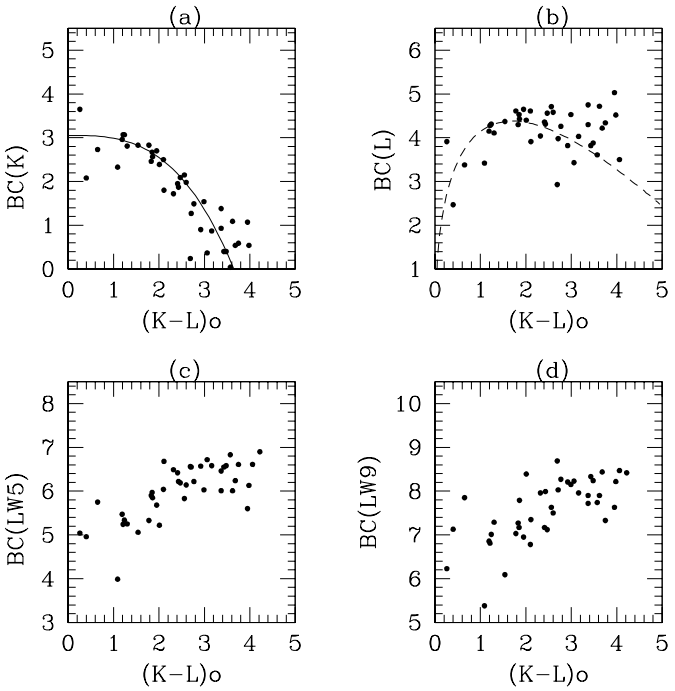

Fig. 5. Dereddened bolometric corrections for near-infrared and ISOGAL bands as a function of the dereddened colour $(K-L)_o$. The continuous line drawn in panel **a)** represents our best fit $BC_K = 3.05 - (K-L)_o^3/20$; the dashed line drawn in panel **b)** represents the fit obtained by WHMc for BC_L.

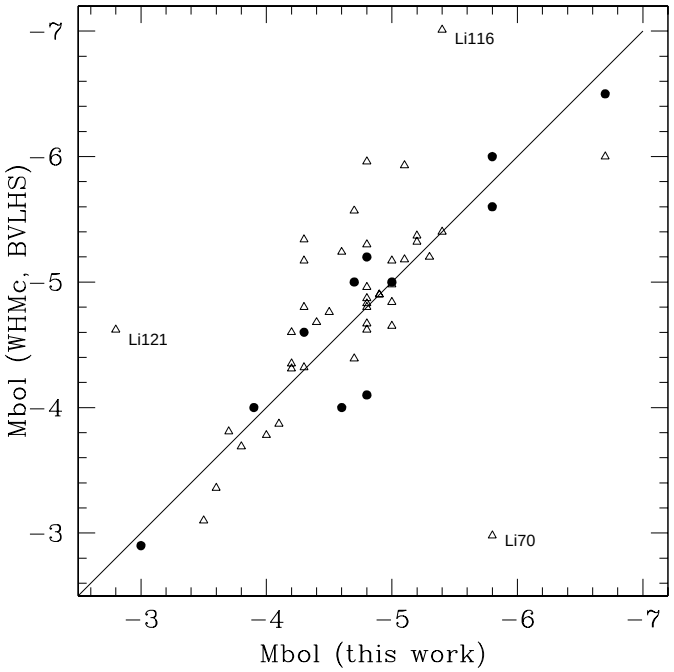

Fig. 6. Comparison between bolometric magnitudes obtained in this work and those obtained by WHMc (triangles) and by BVLHS (circles). For each set of M_{bol} the corresponding photometry ($JHKL$[LW5][LW9] for WHMc; $KL'M$[LW5][LW9] for BVLHS) was used. The objects Li70 and Li121 identified in the figure are discussed in Sect. 8.

using ground-based mid-infrared photometry. The better agreement between BVLHS's results and ours is probably due to the similar method of obtaining M_{bol}. An inspection of Fig. 9 of WHMc reveals that their BC_L relationship is loosely dependent on $(K-L)$, especially if compared to the relationship found in this work. We suggest that M_{bol} is better calculated either by using the bolometric correction for the K band or by integrating the energy distribution, as in BVLHS and in this study.

5. The expansion velocity of the envelope of OH/IR stars: Two distinct populations?

OH/IR stars have been classified in the literature according to their expansion velocity of the OH envelope (Baud et al. 1981; Ortiz & Maciel 1994). Stars that exhibit larger expansion velocity are believed to be younger and more massive, since V_{exp} depends on the luminosity and on the gas-to-dust ratio, which in turn depends on the metallicity (van der Veen 1989; Schutte & Thielens 1989). Luminosity also plays a role but it is difficult to observe the effect caused by each variable separately because populations

of OH/IR have been reported to show wide distributions of luminosity, age, kinematics, etc.

Lindqvist et al. (1992b) studied the kinematics of OH/IR stars near the galactic centre and show that the group with higher expansion velocity of the envelope $V_{\rm exp}$ follows the rotation curve of the Galaxy closer than the low $V_{\rm exp}$ group. BVLHS has presented some evidence that the two groups of OH/IR stars, classified according to their $V_{\rm exp}$, have also different luminosities: almost the whole group with $V_{\rm exp} < 18$ km s^{-1} is fainter than $M_{\rm bol} = -5.0$, whereas the group with $V_{\rm exp} > 18$ km s^{-1} has a broader range of bolometric magnitudes of which half are below –5.0. Sjouwerman et al. (1999) studied the kinematics of OH/IR stars around the Galactic Centre and conclude that the division at $V_{\rm exp} = 16.5$ km s^{-1} is more appropriate.

Here we adopt Sjouwerman's criterion for the objects observed by WHMc and BVLHS and detected in the ISOGAL fields (Tables 3 and 4). Stars are grouped into these two $V_{\rm exp}$ categories as shown in Fig. 7, which can be approximately compared with Fig. 8 of BVLHS. There is no clear distinction between the two groups. It is also possible that the region at the centre of the Galaxy, skipped by ISOGAL, may contain more massive and luminous objects, which would be missing in our statistics, however the more luminous stars listed by BVLHS do not show a sharp concentration at the Galactic Centre. The peak of the distribution of luminosity is, like in BVLHS, at $M_{\rm bol} \simeq -5.0$. The histogram of lower velocity objects reflects the poor statistics for this group, that does not allow us to draw a definitive conclusion on the existence of two distinct groups of OH/IR stars.

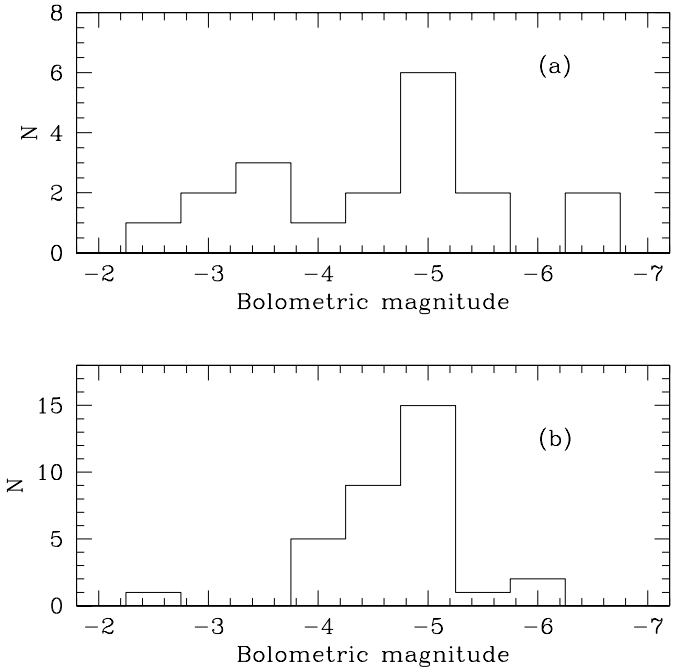

Fig. 7. Histogram showing bolometric magnitudes of OH/IR stars observed by WHMc, BVLHS, and detected in ISOGAL fields, taken from Tables 3 and 4. Stars are separated according to the expansion velocity of the OH envelope: **a)** $V_{\rm exp} < 16.5$ km s^{-1}; **b)** $V_{\rm exp} > 16.5$ km s^{-1}.

6. The K-[LW9] colour

[LW9] is a narrow filter which is not much affected by the 18 μm silicate feature. The $(K-[\mathrm{LW9}])_{\rm o}$ colour is an excellent measure of infrared excess emitted by the envelope, as outlined by Omont et al. (1999c). However, the calculation of mass loss rate is dust model dependent. Figure 8 shows the $(K-[\mathrm{LW9}])_{\rm o}$ × absolute [LW9] diagram of OH/IR stars observed by Lindqvist and ISOGAL taken from Table 3, as well as the predictions of a model for circumstellar dust shells by Groenewegen, already described in Sect. 3. All OH/IR stars are inside the upper part of the region defined by Omont et al. (1999c) where AGB stars showing high mass-loss rates are found. The brightest star found by Omont et al., an OH/IR star identified as IRAS 17382-2830, is also present in this study (Se126), and is at the upper limit of luminosity: $M_{\rm [LW9]} = -13.4$.

Glass et al. (1999) identify AGB stars in the NGC 6522 and Sgr I fields, using the same kind of diagram. In that study, miras extend over a range in colour and magnitude that partially overlaps the box in Fig. 8, but while in Glass et al. the largest value of $(K-[\mathrm{LW9}])_{\rm o} \simeq 3$, the AGB sequence here extends to much redder colours and higher luminosities due to differences between the two samples: the present study addresses OH/IR stars,

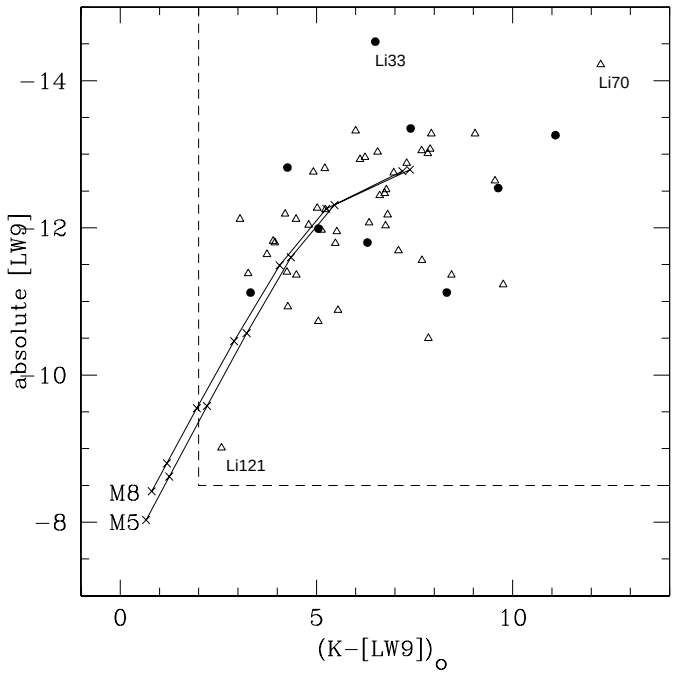

Fig. 8. Colour−absolute magnitude diagram of OH/IR stars observed by WHMc (triangles) and BVLHS (circles), corrected for interstellar extinction. The dotted box marks the region where high mass-loss AGB stars are expected to be found (Omont et al. 1999c) and the lines are model grids by Groenewegen (1993) M5III and M8III spectral types and mass-loss rates in the range 1×10^{-8}–1×10^{-5} $M_{\odot}$/year, with ticks at steps of half a dex.

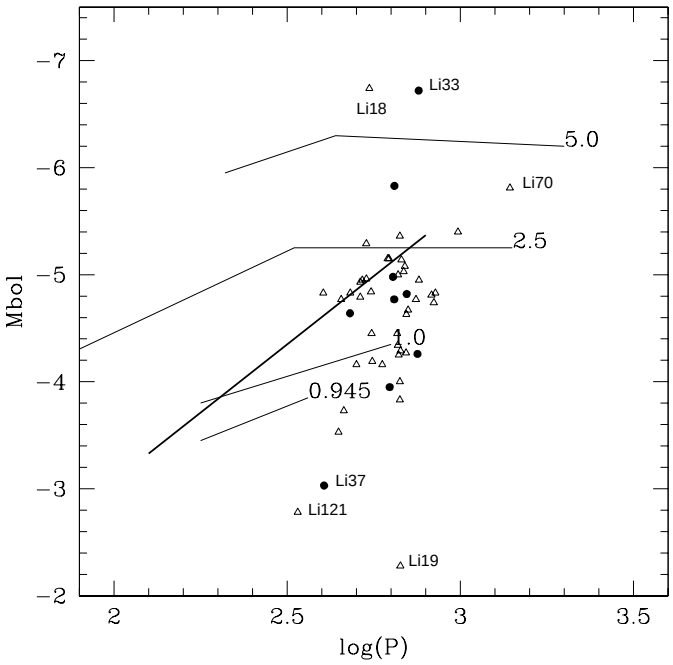

Fig. 9. The period-luminosity relationship for OH/IR stars observed by WHMc and BVLHS, with an ISOGAL counterpart. The thick line represents the relationship derived by Glass et al. (1995) for long period variables in the bulge; thin lines represent masses of the precursors, according to the model by Vassiliadis & Wood (1993) for solar and sub-solar abundances. Bolometric magnitudes are those derived in this paper (Tables 3 and 4). Triangles = WHMc; circles = BVLHS.

whereas the reddest stars of Glass et al. are Miras, which show lower mass-loss rates. They report that no OH/IR stars fall within their fields. Comparing with the grid of models by Groenewegen, one finds that the reddest stars in the study of Glass et al. have mass-loss rates a few times 10^{-7} $M_{\odot}$/year, which marks the onset of the *superwind*, while the ones of the present study can exhibit $\dot{M}$ as high as a few 10^{-5} $M_{\odot}$/year.

As we suggested in Sect. 3, the spread in colour might be partially due to variability in the [LW9] band, since average K magnitudes are considered. The model matches the observations for a great number of sources, however for $(K-[\mathrm{LW9}])_{\mathrm{o}} > 5$ most stars are fainter than the predictions of the model for the [LW9] band, and this discrepancy results in lower luminosities because most of the flux emitted by high mass-loss stars is radiated in the mid-infrared. This interpretation is supported by the deviation of M_{bol} from the luminosity-period relationship (Jones et al. 1994; BVLHS and WHMc) which is discussed in the next section.

7. The period-luminosity relationship

Glass et al. (1995) studied a sample of LPV stars in the bulge (Baade's windows, showing periods up to 700 days. Those stars follow the PL luminosity with the scattering of 0.36 mag which is significantly higher than in the LMC (0.16 mag), mainly because of the finite depth of the bulge. WHMc and BVLHS find that their sample of long period variables very close to the Galactic Centre do not follow any previous PL relationship, the stars showing lower luminosities or, alternatively higher periods than the relationships previously derived. Because bolometric magnitudes have been recalculated with use of mid-infrared photometry which yielded even lower luminosities, we repeated the analysis of WHMc and BVLHS's samples. We take the periods derived by WHMc, van Langevelde et al. (1993) and Jones et al. (1994) and combine them with the bolometric magnitudes described in Sect. 4 in order to study the PL relationship.

Figure 9 shows $\log(P)$ and M_{bol} taken from Tables 3 and 4. Most stars are below the PL line derived by Glass et al. (1995). In the same figure, we plot the grid of models of Vassiliadis & Wood (1993). They give luminosities and periods for a range of initial masses for solar and sub-solar abundances. The small number of objects more luminous than $M_{\mathrm{bol}} = -5.5$ indicates that the initial masses of stars in the sample are rarely higher than $\sim$3 $M_{\odot}$, but they have rather about $1 \sim 2$ $M_{\odot}$, on average. This is incompatible with some of the long periods observed, since it has been shown that the period of a mira increases with its mass (Feast 1963; Feast & Whitelock 1987; Jura & Kleinmann 1992). Besides, that model is intended to reproduce solar to sub-solar metallicity populations, which might not be proper for the central-bulge population. Whitelock et al. (1991) obtain luminosities similar to ours for their sample of IRAS LPV's in the outer bulge.

Note that the very small number of luminous stars in our sample is consistent with the very small number of stars with mass-loss higher than 10^{-5} $M_{\odot}$/year, since there is a correlation between luminosity, initial mass and mass-loss rate (see e.g. Habing 1996 and references therein).

8. Comments on individual objects

Se179 = OH 0.333-00.181 = ISOGAL PJ 174707.0-284442

Se179 (OH 0.333-00.181), Sevenster et al. (1997) detected only one peak at the velocity of –327.2 km s^{-1}. However the detected peak is close to the edge of their velocity coverage, so that a second peak might exist at a more extreme velocity. Se179 is most likely coincident with Sj103 (OH 0.335-0.180) even though the two radio positions differ of $\sim$10″. As shown in Fig. 1 such a difference may well fall within the astrometric uncertainty. In fact, the red peak of Sj103 coincides in velocity with the single peak detected for Se179, while the blue peak is at a velocity of –356.5 km s^{-1}, which is out of the velocity range of the spectrum observed by Sevenster et al. (1997). Only ISOGAL-PJ174707.0-284442 can be associated with the two radio positions: the distances from the ISOGAL source are 10.4 and 1.2″ for Sj103 and Se179, respectively. The ISOGAL source is near the position derived with the ATCA, which is more accurate (Fig. 1). Therefore we

conclude that Sj103 and Se179 are the same maser source and that the position of Sj103 is off by 10″. This very high velocity OH/IR star (–342 km s^{-1}) was first discovered in OH by Baud et al. (1981) (OH 0.3–0.2). Fix and Mutel (1984), observed the radio position with the 10 μm N-band, but did not detect the source and gave an upper limit of <0.6 Jy. BVLHS found two possible counterparts in the K band. ISOGAL-PJ174707.0-284442 is the first mid-infrared counterpart of this high velocity star.

8.1. Infrared bright objects

The following objects are found bright above the ISOGAL AGB branch and hereafter their classification as either foreground objects or as bulge member is discussed:

Li33 = OH 359.762+0.120 = ISOGAL PJ 174435.0-290435

This OH source was detected independently by Lindqvist ($V_{\rm low}$ = −21.0 km s^{-1}, $V_{\rm high}$ = +8.5 km s^{-1}) and Sevenster ($V_{\rm low}$ = −20.6 km s^{-1}, $V_{\rm high}$ = +8.6 km s^{-1}), among others. Its OH emission is very intense, and double-peaked. It was observed by BVLHS in the near and mid-infrared who obtained $(K - L')_{\rm o}$ = 3.65 indicating an optically thick envelope. Van Langevelde et al. (1993) and Jones et al. (1994) independently monitored this source and obtained the period of 758 and 715 days, respectively from radio and infrared observations. There has been some controversy in the literature about the bulge membership of this star. Radio observations show that the OH emission is affected by interstellar scattering that occurs near the Galactic Centre (van Langevelde & Diamond 1991). On the other hand, assuming that this star is really in the bulge, its bolometric magnitude has been evaluated near the limit allowed for AGB stars: $M_{\rm bol}$ = −7.20 (Jones et al. 1994). We find $M_{\rm bol}$ = −6.7, similarly to BVLHS, who finds $M_{\rm bol}$ = −6.5, that makes the location of this star *in* the bulge plausible. This OH source has an IRAS counterpart (IRAS 17413-2903) at 1.5 error ellipse far from the radio position. Its mid-infrared magnitudes indicate that the IRAS-ISOGAL sources refer to the same object: [6.8 μm] = +1.74, [12 μm] = +1.10 [1], [14.9 μm]= +0.27.

Li18 = OH 359.640-0.084 = ISOGAL PJ 174505.3-291713

Like the previous star (Li33), Li18 has a $M_{\rm bol}$ = −6.7 and is positioned quite above the PL relationship (Fig. 9). WHMc report a period of 546 days and $M_{\rm bol}$ = −6.0. Its high radial velocity, −142.3 km s^{-1}, however, suggests a bulge membership.

Se145 = OH 359.149-00.043 = ISOGAL PJ 174345.0-294101

This source was detected by Sevenster ($V_{\rm low}$ = +34.9 km s^{-1}, $V_{\rm high}$ = +39.3 km s^{-1}). Such an extremely small ΔV suggests interstellar emission. It is a very red object ([LW5]−[LW9] = 2.72), but because the [LW5] and [LW9] observations were not simultaneous this colour index might have been affected by variability. There is an IRAS counterpart (IRAS 17405-2939) 0.4 error ellipse far from the OH position and ISOGAL and IRAS magnitudes are compatible: [6.8 μm] = +1.97, [12 μm] = +0.08, [14.9 μm] = −0.75. Its small velocity is compatible with a foreground disk object, but additional infrared observations are necessary to confirm its YSO nature and determine its distance.

Se151 = OH 359.117-00.169 = ISOGAL PJ 174409.9-294639

This object was detected by Sevenster ($V_{\rm low}$ = −109.6 km s^{-1}, $V_{\rm high}$ = −67.3 km s^{-1}) and corresponds to IRAS 17409-2945. Its magnitudes are compatible with one another: [6.8 μm] = +2.34, [12 μm] = +1.52, [14.9 μm] = +1.02, and [25 μm] = −0.2. Its colours, ΔV, and OH spectrum are typical of an OH/IR star, but near-infrared data are needed to derive its luminosity and to confirm its bulge membership, which is suggested by its large velocity.

Li70 = OH 359.971-0.119 = ISOGAL PJ 174601.1-290124

It is a double-peaked OH source detected by Lindqvist ($V_{\rm low}$ = −27.8 km s^{-1}, $V_{\rm high}$ = +10.8 km s^{-1}). Despite its bright ISOGAL magnitudes ([6.8 μm] = +2.30, [14.9 μm] = +0.68), it was not detected by IRAS. It was observed by WHMc (K = 14.79) and BVLHS (K > 14). It is the reddest object of this study: $(K - L)_{\rm o}$ = 4.22, $(K - L')_{\rm o}$ = 7.44, $(K-[{\rm LW9}])_{\rm o}$ = 12, however [LW5]−[LW9] = 1.62 is just moderate. Van Langevelde et al. (1993) monitored it in OH radio frequencies and obtained the period of 1391 days. If the object is really in the bulge, it is one of the brightest: from WHMc *and* from BVLHS near-infrared data, in combination with ISOGAL data, we obtain the same result: $M_{\rm bol}$ = −5.8. On the other hand from their near infrared data WHMc find it much fainter ($M_{\rm bol}$ = −2.98), while BVLHS finds $M_{\rm bol}$ = −6.0 using near-infrared data and N band photometry, which is consistent with our result. The high $(K-L)_{\rm o}$ value suggests a high mass-loss rate and an optically thick envelope (no counterpart is reported by WHMc in J or H bands). We suggest that its location in the bulge might be compatible with its magnitude and luminosity.

8.2. Very red ISOGAL objects: ([LW5]–[LW9]) > 3

Li3 = OH 359.429+00.036 = OH 359.429+0.035 = ISOGAL PJ 174406.9-292417

The OH source was independently detected by Lindqvist et al. and Sevenster et al., and it has a peculiar OH spectrum. There are two strong peaks at $V_{\rm low}$ = −10.8 km s^{-1} and $V_{\rm high}$ = +17.6 km s^{-1}, and a broad emission feature at $V \simeq 0$ km s^{-1}. It has the reddest ([LW5]–[LW9]) colour of the sample, but there are neither WHMc nor BVLHS observations, nor an IRAS detection for this source. Considering the colour index and the

[1] The IRAS zero-magnitude fluxes considered are those in the *IRAS Explanatory Supplement*, i.e. 28.3, 6.73, 1.19, and 0.43 Jansky for the 12, 25, 60, and 100 μm bands, respectively.

OH spectrum we suggest that this object might be a post-AGB star or a YSO.

Sj31 =OH 359.936-00.145 = ISOGAL PJ 174602.8-290359

Sjouwerman et al. (1998) point out that the second OH peak, at $v = +13$ km s^{-1}, is very faint and it cannot be confirmed. Consequently, there is a considerable chance that the OH emission is of interstellar origin. Its red colour is very reliable since ISOGAL magnitudes were obtained at the same epoch.

Li111 =OH 000.319-00.041 = OH 0.319-0.040 = ISOGAL PJ 174632.2-284104

This OH source was detected by Sevenster ($V_{\rm low} = +56.8$ km s^{-1}, $V_{\rm high} = +93.3$ km s^{-1} and Lindqvist ($V_{\rm low} = +57.3$ km s^{-1}, $V_{\rm high} = +92.2$ km s^{-1}). van Langevelde et al. monitored it in radio, but no fit of a regular period curve was possible. The existence of a third peak in the OH spectrum as well as the very high ([LW5]–[LW9]) colour and the lack of regular period suggests this object is either a young stellar object or a post-AGB object. It was not observed by WHMc and BVLHS did not detect any near-infrared counterpart in K and L' bands. The interstellar extinction in its direction is about 29 mag. If this object is as red as the most extreme ones in Fig. 8, it would have $K - [\mathrm{LW9}] \simeq 10$, which gives $< K > \simeq 15$. Such a faint magnitude is characteristic of evolved post-AGB stars and YSO's.

Li96 = OH 0.173+0.211 = ISOGAL PJ 174512.5-284044

Despite the large value of [LW5]−[LW9]= 3.23, it has only moderate values of $(K-L)_{\rm o} = 2.01$ and $(K-[\mathrm{LW9}]_{\rm o}) = 6.00$. Its nature as an AGB star is well established from the period of 514 days of its light curve.

8.3. Low-luminosity stars: $M_{bol} > -3.0$ ($L < 1.3 \times 10^3\ L_\odot$)

Li37 = OH 359.776-0.120 = ISOGAL PJ 174533.3-291123

It is one of the strongest OH emitters, its OH spectrum looks like a well-defined double-peak. We obtain $M_{\rm bol} = -3.0$; Jones et al. (1994) evaluates $M_{\rm bol} = -3.40$, however they do not find a regular period from the L-band light curve. BVLHS found $M_{\rm bol} = -2.9$. Van Langevelde & Diamond (1991) and Frail et al. (1994) demonstrated that the OH source is located in the Galactic center region, behind the scattering screen. We conclude that this object is a non-variable/irregular OH/IR star, near the faint end of the AGB branch (see also discussion in BVLHS).

Li121 = OH 0.452+0.046 = ISOGAL PJ 174630.7-283131

This object has typical characteristics of a mira-type star. All its colour indices are low (e.g. $(K-[\mathrm{LW9}])_{\rm o} = 2.58$), and its $(K-L)_{\rm o}$ is the bluest in the WHMc's sample: $(K-L)_{\rm o} = 0.26$. Its position in the $(K-[\mathrm{LW9}])_{\rm o} \times M_{[\mathrm{LW9}]}$ diagram (Fig. 8) suggests that it has the lowest mass-loss rate among the stars measured in the near-infrared and by ISOGAL. According to Groenewegen's models the mass-loss rate does not exceed $1 \times 10^{-7}\ M_\odot$/year. The extinction-corrected absolute magnitude is $M_K = -6.4$, which is faint for an optically thin envelope AGB star. This suggests that WHMc overestimated the luminosity of this star: $M_{\rm bol} = -4.62$ (WHMc); $M_{\rm bol} = -2.8$ (this work; however the value of $BC_K = 3.65$ that we derived is surprising). The period is also the shortest in the sample: 339 days, comparable to *o* Ceti. Other miras showing 1612 MHz OH emission have been previously reported in the literature: te Lintel Hekkert et al. (1989) list many miras as counterparts of OH sources in the solar neighbourhood, however the observed intensity of the OH emission in such a star at the distance of the bulge would be exceptional.

Li19 = OH 359.652-0.131 = ISOGAL PJ 174518.1-291804

We find $M_{\rm bol} = -2.3$, similarly to WHMc who find $M_{\rm bol} = -1.68$. Differently from the former sources, this star has an optically thick envelope and a long period of 671 days. Like OH 0.452+0.046, the absolute K magnitude is far too faint for an AGB star. For its $(K-L)_{\rm o} = 3.06$ colour index, Lepine et al. predict $M_K = -6.7$, which is much brighter than $M_K = -2.65$ found for this star. We suggest that this star is located *behind* the bulge.

Li107 = OH 0.261-0.143 = ISOGAL PJ 174647.9-284715

This star has also an optically thick dust shell, considering its $(K-L)_{\rm o} = 2.69$ color index. Its $M_{K\rm o} = -2.92$ and bolometric magnitude ($M_{\rm bol} = -1.45$, WHMc; $M_{\rm bol} = -2.7$, this work) are too faint and incompatible with its colour index. Infrared monitoring carried out by WHMc revealed no period, but it has shown small-amplitude variability. This fact, as well as its triple peaked OH spectrum suggest that it might be a young stellar object.

9. Conclusions

The ISOGAL survey in the inner part of the bulge has found infrared counterparts of OH maser sources for almost 100% of the cases, amounting to 110 objects. The mass-loss rates calculated using the grid of models by M. Groenewegen for circumstellar envelopes are in the range 3×10^{-7} up to a few times $10^{-5}\ M_\odot$/year. However the sources display a considerable spread in the $(K-[\mathrm{LW9}])$ colour when compared with the predictions of the models, which is probably caused by variability.

OH/IR stars in the bulge show a wide distribution of luminosity, peaked at $8 \times 10^3\ L_\odot$ ($M_{\rm bol} = -5.0$), and with very few stars more luminous than $1.5 \times 10^4\ L_\odot$ ($M_{\rm bol} < -5.6$). Only a minor fraction of OH/IR stars have thus initial masses larger than $\sim 3\ M_\odot$.

The luminosities of OH/IR stars in this study lie practically all well below the PL relationship, as previously

found by Wood et al. (1998) and BVLHS, and even further below than Wood et al.'s values.

We do not find clear evidence of two distinct populations of OH/IR stars in our sample, classified according to their expansion velocity of the envelope, as suggested by others (BVLHS, Sevenster et al. 1995).

Acknowledgements. This work was carried out in the context of EARA, the European Association for Research in Astronomy. R. Ortiz thanks "Conselho Nacional de Desenvolvimento Cientifico e Tecnologico" (CNPq, Millennium Institute PADCT III no. 62.0053/01-1 and PRONEX; Brazil) and "Nederland Organisatie voor Wetenschappelijk Onderzoek" (NWO, The Netherlands). The authors acknowledge the valuable discussions with C. Alard, C. Loup, M. Sevenster, L. Sjouwerman, and J. van Loon.

References

Baud, B., Habing, H. J., Matthews, H. E., & Winnberg, A. 1981, A&A, 95, 156
Bertoldi, F., Timmermann, R., Rosenthal, D., Drapatz, S., & Wright, C. M. 1999, A&A, 346, 267
Blommaert, J. A. D. L. 1998, ISOCAM Photometry Report, `http://www.iso.vilspa.esa.es`
Blommaert, J. A. D. L., van der Veen, W. E. C. J., & Habing, H. J. 1993, A&A, 267, 39
Blommaert, J. A. D. L., van der Veen, W. E. C. J., van Langevelde, H. J., Habing, H. J., & Sjouwerman, L. O. 1998, A&A, 329, 991 (BVLHS)
Césarsky, C., Abergel, A., Agnese, P., et al. 1996, A&A, 315, L32
David, P., & Papoular, R. 1990, A&A, 237, 425
David, P., & Papoular, R. 1992, A&A, 265, 195
Epchtein, N., and the DENIS scientific team 1997, The Messenger, 87, 27
Feast, M. 1963, MNRAS, 125, 27
Feast, M., & Whitelock, P. A. 1987, in The late stages of stellar evolution, ed. S. Kwok, & S. R. Pottasch, 33
Feast, M., Glass, I. S., Whitelock, P. A., & Catchpole, R. M. 1989, MNRAS, 241, 375
Frail, D. A., Diamond, P. J., Cordes, J. M., & van Langevelde, H. J. 1994, ApJ, 427, L43
Frogel, J. A., & Whitford, A. E. 1987, ApJ, 320, 199
Glass, I. S., Whitelock, P. A., Catchpole, R. M., & Feast, M. W. 1995, MNRAS, 273, 383
Glass, I. S., Ganesh, S., Alard, C., et al. 1999, MNRAS, 308, 127
Glass, I. S. 1999, in Handbook of Infrared Astronomy (Cambridge University Press)
Groenewegen, M. 1993, Ph.D. Thesis, University of Amsterdam
Groenewegen, M. 1997, in The Impact of Large Scale Near-IR Surveys, ed. F. Garzón, N. Epchtein, A. Omont, & B. Burton (Kluwer Academic Press), 165
Habing, H. J. 1996, A&AR, 7, 97
Harvey, P. M., Bechis, K. P., Wilson, W. J., & Ball, J. A. 1974, ApJS, 248, 331
Jones, T. J., McGregor, P. J., Gehrz, R. D., & Lawrence, G. F. 1994, AJ, 107, 1111
Jura, M., Kleinmann 1992, ApJS, 79, 105
Koornneef, J. 1983, A&A, 128, 84
Lépine, J. R. D., Ortiz, R., & Epchtein, N. 1995, A&A, 299, 453
Le Squeren, A. M., Sivagnanam, P., Dennefeld, M., & David, P. 1992, A&A, 254, 133
Lewis, B. M., & Engels, D. 1993, MNRAS, 265, 161
Lindqvist, M., Winnberg, A., Habing, H. J., & Matthews, H. E. 1992a, A&AS, 92, 43
Lindqvist, M., Habing, H. J., & Winnberg, A. 1992b, A&A, 259, 118
Lutz, D., Feuchtgruber, H., Genzel, R., et al. 1996, A&A, 315, L269
Lutz, D. 1999, in The Universe as seen by ISO, ed. P. Cox, & F. Kessler, ESA SP-427, 623
Monet, D., et al. 1998, The PMM USNO-A2 Catalogue, US Naval Observatory Flagstaff Station
Omont, A., & The ISOGAL collaboration 1999a, in Astrophysics with Infrared Surveys: a prelude to SIRTF, Pasadena, ASP Conf. Ser., 177, 261
Omont, A., & The ISOGAL collaboration 1999b, in The Universe as seen by ISO, ed. P. Cox, & M. F. Kessler (ESA Special Publications series), SP-427
Omont, A., Ganesh, S., Alard, C., et al. 1999c, A&A, 348, 755
Omont, A., & The ISOGAL collaboration 2002, in preparation
Ortiz, R., & Maciel, W. J. 1994, A&A, 287, 552
Pérault, M., Omont, A., Simon, G., et al. 1996, A&A, 315, L165
Rohlfs, K., & Kreitschmann, J. 1987, A&A, 178, 95
Schuller, F., & The ISOGAL collaboration 2002, in preparation
Schultheis, M., Ganesh, S., Simon, G., et al. 1999, A&A, 349, L69
Schutte, W. A., & Tielens, A. G. G. M. 1989, ApJ, 343, 369
Sevenster, M. N., Dejonghe, H., & Habing, H. J. 1995, A&A, 299, 689
Sevenster, M. N., Chapman, J. M., Habing, H. J., Killeen, N. E. B., & Lindqvist, M. 1997, A&AS, 122, 79
Simon, G., & The DENIS collaboration 2002, in preparation
Sjouwerman, L. O., van Langevelde, H. J., Winnberg, A., & Habing, H. J. 1998, A&AS, 128, 35
Sjouwerman, L. O., Habing, H. J., Lindqvist, M., van Langevelde, H. J., & Winnberg, A. 1999, in The central parsec, ASP Conf. 184, ed. H. Falcke, A. Cotera, W. J. Duschl, et al.
te Lintel Hekkert, P., Versteege-Hensel, H. A., Habing, H. J., & Wiertz, M. 1989, A&AS, 78, 399
van de Hulst, H. C. 1949, Rech. Astr. Obs. Utrecht 11, Part 2
van der Veen, W. E. C. J., & Habing, H. J. 1988, A&A, 194, 125
van der Veen, W. E. C. J. 1989, A&A, 210, 127
van Langevelde, H. J., & Diamond, P. J. 1991, MNRAS, 249, 7P
van Langevelde, H. J., Janssens, A. M., Goss, W. M., Habing, H. J., & Winnberg, A. 1993, A&AS, 101, 109
van Loon, J. T., Groenewegen, M. A. T., de Koter, A., et al. 1999, A&A, 351, 559
Vassiliadis, E., & Wood, P. R. 1993, ApJ, 413, 641
Whitelock, P., Feast, M., & Catchpole, R. 1991, MNRAS, 248, 276
Wood, P. R., Habing, H. J., & McGregor, P. J. 1998, A&A, 336, 925 (WHMc)